UNIVERSITY OF TWENTE.

Faculty of Electrical Engineering, Mathematics & Computer Science

Design of a Flat-Swipe Finger Vein Recognition Device in the NIR Spectrum

Roberto Prieto Alvarez
B.Sc. Thesis
May 2020

Supervisors:
dr. ir. L. J. Spreeuwers
ing. G.L. Laanstra
dr. ing. E.A.M. Klumperink

Data Management & Biometrics Group
Faculty of Electrical Engineering,
Mathematics and Computer Science
University of Twente
P.O. Box 217
7500 AE Enschede

Design of a Flat-Swipe Finger Vein Recognition Device in the NIR Spectrum

Roberto Prieto Alvarez, EEMCS, The University of Twente, the Netherlands

***Abstract*—A new approach is made as an alternative to existing technologies to obtain Near Infrared (NIR) finger vein images. The new implemented technique is done with the use of a line-scan charged couple device. The scanning process consists of a finger sliding perpendicularly to a line sensor, coated with an infrared-pass filter and an illumination technique of LTM (Light Transmission Method). It was found that this technique is viable to acquire some vascular features of fingers in the NIR spectrum. Contrast, resolution and vertical displacement tests show that the requirements for finger vein image obtainment are met by this procedure. The results exhibit knuckles and veins which shows a direct consistency with respect to the real spatial position in the finger. Therefore proving this technology as a candidate for future finger vein imaging.**

I. INTRODUCTION

BIOMETRIC security systems play an important role in digital recognition and security. Passwords are the most common way of biometric authentication [1]. The growth of demand in security and online services makes remembering passwords a complicated process [2]. The user must remember and update regularly these passwords. With the growth of biometric authentication, some might argue that passwords are obsolete and they should give place to biometric authentication [3]. The biometrical data from the human body varies from person to person. This data provides exclusive access and authorization from the user to a specific application. There are very secure methods available and implemented in smartphones and other end-user available devices. Some biometrical security systems are not capable to distinguish between the legitimate user and an accurate representation. Some examples of this category of devices are a twin in case of face recognition or a fake finger in case of a fingerprint scanner [4]. It has been shown that one of the hardest biometric patterns to imitate is the vascular distribution inside the human body [5]. The vascular vessels are distributed in a unique manner that varies from person to person. There are existing techniques for scanning the patterns of these vessels. These scanners tend to be relatively big, intimidating and expensive [5].

In this paper, the design, development and assessment of flat finger vein scanner is made with specific attention given to a decrease in size. The aim of this work is to develop a cost-effective basis towards a new technology investigation. The physical working principle of this new device will be based on some of the already existing technologies and findings. The most important one is the different absorption coefficient of hemoglobin around other tissues under a NIR environment. This produces a light contrast effect that can be recorded by a proper imaging device.

In Section II, the design proposal will be evaluated based on the existing congruent technologies. Section III describes the guidelines that the design must comply with from a cursory point of view. Thereupon in Section IV describes the chosen approach in detail, followed by Section V where results of the experiments are shown. Finally Section VI comments on the results and Section VII draws conclusions from them.

II. RELATED WORK

There are already finger vein recognition devices commercially available. Some of them are affordable to the end user while others are more costly. These devices are characterized by obtaining a false acceptance rate of, for example, 1 out of 10000 and a false rejection rate of 1 in 100. This technology has improved over the years and it is gaining more popularity due to its difficulty of replication. Therefore attaining a high security level. Although there is existing research in the field of biometrics, the amount is far less than the fingerprint technology. This is due to the higher relative difficulty of obtaining finger vein patterns when compared to fingerprints [5].

Most of the existing work related to finger vein recognition devices consists of a finger illuminated by a NIR light projecting the information on a optical sensor mounted on a lens and a NIR filter. This approach gives outstanding results but has its limitations. There might be an approach that covers those limitations while still produces similar results. In this section, the existing approaches are investigated, highlighting its relevant characteristics.

A. Devices already available

As mentioned before there are already commercially available sensors with good performance. Also it was mentioned that fingerprint scanning technologies are more developed. This advantage needs to be exploited since both finger vein and finger print technologies share some common characteristics. These potential characteristics, among others, are: size, portability, power consumption, speed and liability. These are discussed further in detail:

1) Finger vein devices: The company Hitachi Ltd. leads the market in commercial applications. There are a wide variety of options, such as the ”Hitachi H1 Finger Vein Reader”, a USB accessible device. Hitachi also claimed in 2009 the successful development of a 3mm-thick-flat finger vein

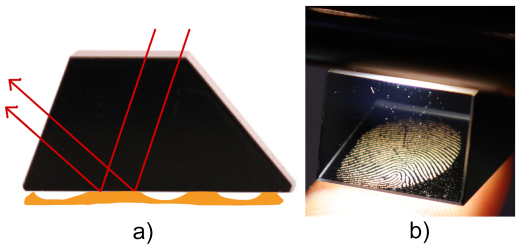

Fig. 1. The optic-fingerprint sensor consists of a prism, a small lens and an image sensor. a) The surface touching the prism reflects incident light out of the prism. b) The fingerprint makes reflects incident light on the prism only on the contact points, i.e. fingerprint.

scanner with integrated micro lens array, NIR filter and sensor [6]. But this all-in-one solution has not seem to be available nor seen anywhere commercially. Secondly, another more reliable method is a so called angiogram scan. This method introduces a contrast agent in the blood that can be seen as a shadow in an X-ray image. This method is used uniquely in the medical field. It does not fall within the requirements of a portable, flat finger vein scanner. Apart from Hitachi Ltd. there are other commercially available sensors but mostly all of them make use of the same principle. The hemoglobin and its NIR characteristics in contrast to surrounding tissue. These sensors are provided, among others, by YannanTech or Mofiria [5]. Research of finger vein recognition is also being done at several universities such as the devices developed by the Civil Aviation University of China [7], Norwegian Biometrics Laboratory [8] or the University of Twente [9]. One of the advantages of these devices is that they are normally open sources thus enabling the community of biometrical scientists to compare and replicate experiments.

2) Fingerprint devices: Due to the increased maturity of this biometric recognition method, intense research has been made. The predominant technology for obtaining fingerprints is by means of a capacitive array [10]. Ultra thin camera-integrated devices for fingerprint imaging have already been developed [11]. There are also optical fingerprint devices that use a prism lens to project an image of surface contact on an optic sensor. During the research stage of this project such a device was obtained and disassembled. The prism reflects to the optic sensor only the contact points, as shown in Figure 1-B therefore this method was later discarded. An image of this prism is shown in Figure 1. Lastly, another solution available are the swipe fingerprint sensors. It consists of a cmos sensor which produces successive images. These images are then stacked on a 2D-depth matrix producing a 3D model of the fingerprint [12]. A commercial product image is shown in Figure 2.

B. Addressing the issue

The development of a swipe, flat finger vein scanning technology can only be done by analyzing the existing techniques applied to finger biometrics mentioned above. Hitachi's claimed 3mm sensor and the Swipe fingerprint capacitive sensors can lead to the approach of a flat line optical sensor.

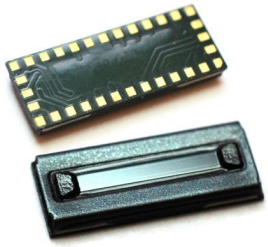

Fig. 2. A top and bottom view of a commercial fingerprint swipe sensor [12].

The potential characteristics of the final device after further extensive research are:

- Already available technology: Line sensors are widely available due to its large involvement on bar code scanners.
- The size of such device is small compared to the existing devices.
- Low cost due to the largely commercialized components.

Hereafter this paper describes the process of design, implementation and testing of a flat-swipe-optical-line sensor as a viable technology to detect finger veins. It will consist of a line-optic sensor where the finger will slide on top, thus producing the desired images.

III. DESIGN CRITERIA

During the design process it is crucial to set some requirements for the device. It has to be noted that some of the requirements are more important than others. The final prototype aims to satisfy, withing the possibilities, most of them. In this section the main parameters will be established according to the criteria stated. These are the criteria related with the line sensor, criteria of the used hardware and criteria of the software.

A. Sensor Criteria

1) Size: Setting the width of the finger as a minimum length of the sensor allows getting full image of the total width of the finger. This distance varies depending on age, ethnics and more. Studies suggest that the average adult index finger width is $20.3\,\mathrm{mm}$ [13]. Thus the minimum length of the active pixel area must be at least $20.3\,\mathrm{mm}$. A smaller pixel size means less light impacting the sensor, which translates in darker images. Commercial sensors in smartphones or in full-frame cameras have a pixel size from$1\,\mu\mathrm{m}$ to $6\,\mu\mathrm{m}$ [14]. Anything on the higher end should be sufficient for the pixel width of the line sensor. This is based on the fact that the already existing finger vein recognition devices use this size of sensors. Since the objective of this assignment is to make a much smaller and compact design of a finger vein device, the height of the line sensor must also have a limit, which arbitrary falls to a range of between $5\,\mathrm{mm}$ to $1\,\mathrm{cm}$.

2) Coating: Advanced camera optic sensors have coating, piezoelectric and filters to protect the sensor and filter unwanted light wavelengths. This is partially due to some lenses causing unwanted reflections in the IR spectrum on the sensor

and partially to protect the sensor from dust and scratches. Such filter is unwanted in this case since IR is the only target frequency. On the other hand, swiping the finger on the sensor would scratch it and make it non-functional with time. Having coating creates distance from the sensor and the optical image, which introduces unwanted blur and might lead to double-imaging. Therefore the sensor is desired to be factory filter-less and possibly without any kind of coating.

3) NIR responsivity: Hemoglobin in the blood has a different absorption coefficient than the surrounding tissues. This is the principle used in most optical vessel recognition devices. The subject's finger will be lit by an IR light. A filter is to be placed on top of the sensor avoiding unwanted light frequencies on the sensor. It has been found that the optimal light wavelength for finger imaging is $850\,\mathrm{nm}$ [15]. Therefore the line sensor must meet this criteria and be responsive to this particular wavelength.

4) CCD or CMOS: The main question is Global Shutter (CCD) or Rolling shutter (CMOS). Rolling shutter would induce shifting on one side of the image due to the moving subject (finger sliding). Therefore rolling shutter is not a good option, descarting CMOS. On the other hand, under an overexposed circumstance, CCD sensors show smearing. CCDs in general are more light responsive due to its larger pixel size. Taking both drawbacks and advantages into account, the line sensor chosen must be a CCD.

5) Functionality: Due to a moving target being scanned (finger swiping), a high frame rate (line-rate) is desired. As a reference, it is expected a swiping velocity of around $1cm/s$. The expected size of the smallest visible vein is around $0.5\,\mathrm{mm}$. In order to see a vein, it must be 2 pixels in width. Equation 1 gives the minimum required frame rate.

$$f_{minimum} = \frac{v_{finger}}{s_{vein}/2} \tag{1}$$

Substituting the required values in Equation 1 yields the required frame rate of 40 lines/second. Following the same criteria of the smallest visible vein, a resolution requirement can also be drawn. An equation giving the minimum required resolution can be seen in Equation 2.

$$R_{minimum} = \frac{w_{finger}}{s_{vein}/2} \tag{2}$$

The resulting minimum resolution using Equation 2 is 92 pixels. A higher resolution will indeed give more reliable results.

B. Hardware Criteria

Aiming for simplicity and a small-sized sensor, yields to use the minimum additional hardware. The hardware chosen cannot depend on different supply voltages than the micro-controller, such as the supply voltage and the operating voltage of the components. A good approach is to rely directly on the power from a USB port; yielding to a new requirement. For the illumination of the finger, NIR LEDs will be used. Having a peak on its spectral response at $850\,\mathrm{nm}$ is a requirement.

C. Software Criteria

C is the first choice in programming languages for embedded systems given its ability to access low level hardware [16]. The design of this prototype aims to be future-proof and leaving a good environment for future improvement. Higher available processing power translates into larger opportunities in the future for implementing image processing on board the device.

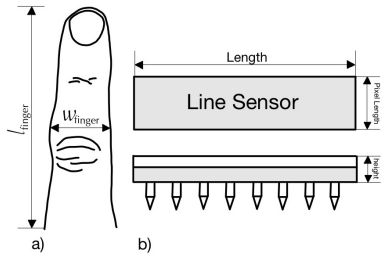

Fig. 3. a) Illustrative top view of a finger, perpendicular to the sensor, in the swiping direction. b) Top and cross sectional view. On the top view the sensor is shown with length and width. On the side view the NIR filter is shown in white and the sensor grey.

D. Parameters summary

For simplification purposes, a list with all the summarized requirements discussed previously is shown below. The list presents the eight most important characteristics.

- Size: minimum effective length of $20.3\,\mathrm{mm}$. Height of sensor from $5\,\mathrm{mm}$ to $10\,\mathrm{mm}$.
- Coating: no filters added on top of the sensor.
- NIR responsive to $850\,\mathrm{nm}$.
- Charge Couple Device
- Performance: minimum of $40\ lines/second$ and resolution of minimum 92 pixels.
- Minimum Additional Hardware: all elements of the device running on the same voltage.
- LEDs for illumination at around $850\,\mathrm{nm}$.
- Programmed in C for embedded systems.

IV. IMPLEMENTATION

Referring to the requirements in the "Design Criteria" section, the device aims to meet most of them. The process outcome is a line-scan CCD driven by a micro-controller delivering images in the NIR spectrum of a finger. The final prototype is shown in Figure 9. Two areas of interest have been divided within the implementation: hardware solution and the software solution.

A. Hardware

The chosen CCD line sensor is the TCD1304DG manufactured by Toshiba. The size of this device is $41.6\,\mathrm{mm}\pm0.5\,\mathrm{mm}$ (length) by $9.65\,\mathrm{mm}\pm0.3\,\mathrm{mm}$ (width) by $7.22\,\mathrm{mm}\pm0.5\,\mathrm{mm}$ (height). The spectral responsivity of this CCD is around 30% of its maximum response (located at $550\,\mathrm{nm}$) at the desired wavelength of $850\,\mathrm{nm}$. A graph of its spectral responsivity is shown in Figure 4. The absolute maximum line rate output

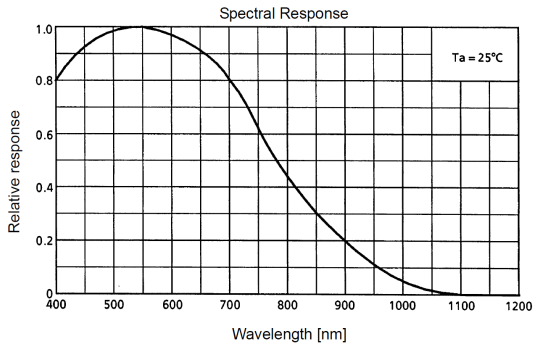

Fig. 4. Spectral responsivity of the chosen CCD. Showing a maximum at $550\,\mathrm{nm}$) and 30% of the normalized maximum responsivity at $850\,\mathrm{nm}$, the desired wavelength [17]

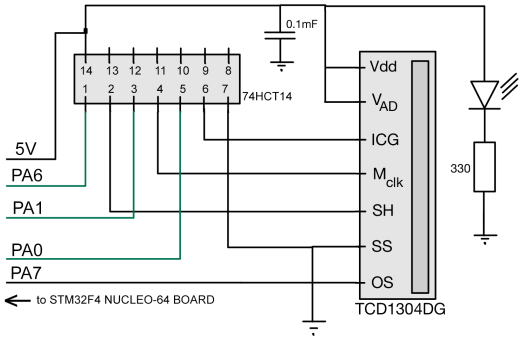

Fig. 5. Wiring schematic of the line sensor (TCD1304DG) with the schmitt trigger and the lines (green) of the STM32F4 board (omitted for simplification)

is 270 $lines/second$, according to the datasheet. In addition, the smallest integration time is $1/100000$. The resolution is 3694 pixels distributed in a series making a total of $29.1\,\mathrm{mm}$, which translates in a pixel size of $8\,\mu\mathrm{m}$ by $200\,\mu\mathrm{m}$. The sensor is coated with a glass surface, which is not optimal. The price of this chip varies around 25 $. This chip offers the possibility of modifying parameters such as the exposure and integration time. Although the chip's operating voltage ranges between $3V$ and $5.5V$, the sensitivity response suggests that greater sensitivity will be obtained at $5V$ ($225\ V/lx \cdot s$) rather than at $3V$ ($100\ V/lx \cdot s$) [17].

The chosen micro-controller for driving the CCD and reading the signal from it operates at 3.3V. A Schmitt trigger at 5V was used between the micro-controller and the clock lines of the CCD. A coupling effect was found between the output lines of the micro-controller, as well as overshoot in both rising-edges and falling-edges. They were both mitigated by the Schmitt trigger. Figure 5 shows a schematic of the design, where the Schmitt trigger is placed between the output lines of the micro-controller and the CCD. The analog sample-and-hold output of the CCD is read directly by the ADC of the micro-controller.

An aperture filter of a width of $0.5\,\mathrm{mm}$ was placed directly above the glass coating of the CCD. This only allows light coming perpendicularly to the sensor. The filter was hand-crafted by using a blade on a piece of magnetic tape. This filter can be visualized as the right-most element in Figure 9. The LED illuminating the finger has a spectral response with peak wavelength is at around $860\,\mathrm{nm}$. Illumination intensity was controlled by reducing the current with a potentiometer. The illumination chosen method is transmission, resulting in high-contrast vascular pattern images [5].

An acrylic IR filter was placed on top of the aperture filter. This filter blocks any visible light from $750\,\mathrm{nm}$ and below. The filter only allows light in the NIR spectrum to hit the sensor, therefore making it an optimal solution for blocking undesired environmental light. A spectral response of this filter is shown in Figure 6. The implementation of this filter can be seen as the middle element in FIgure 9.

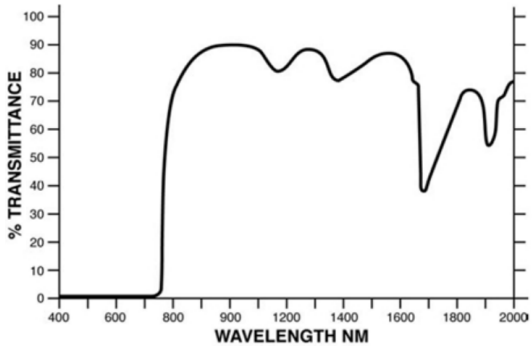

Fig. 6. Spectral responsivity of the IR filter. The area of interest is $850\,\mathrm{nm}$ which shows an approximate transmittance of 90% [18].

The micro-controller chosen for driving and performing data acquisition was included in the STM32F4 Nucleo-64 board. This board features an ARM Cortex-M4 core, several timers, multi-channel ADC, full peripheral access DMA and several communication protocols available, such as USART and SPI.

B. Software

The software programmed into the STM32F401RE micro-controller was written in embedded C. Portability between devices from the STM family and full control of the hardware were the two of the reasons behind choosing this programming language. The software was made from zero, without external libraries, addressing the registers of the chip directly. This is a complicated process but it allows flexibility and gives full control of the hardware. The CPU intervention is negligible. Thus leaving room for future CPU-intense tasks such as image processing or control. The software is divided in several functional blocks, shown in Figure 7.

1) Driving the CCD: Pulse timing requirements in the CCD require use of timers in the microcontroller, specialized timing clocks used to measure time intervals. A total of 4 timers were used. One timer as the master and 3 timers as the slaves. These timers are shown in the top area of Figure 7. Timer4 acts as a clock master while Timer2, Timer3 and Timer5 as slaves. This hierarchy was implemented to ensure that all timers start and step at the same instant, i.e. on the master trigger. This master timer was needed since it takes some time for the compiler to execute one line of code before jumping to the next one. Thus inducing a delay between timers. By starting Timer4, all of the slaves at the same time with a zero delay. The CCD has 3 control lines, SH (Shift Gate), ICG (Integration Clear Gate) and CLK (clock line). SH controls the exposure time,

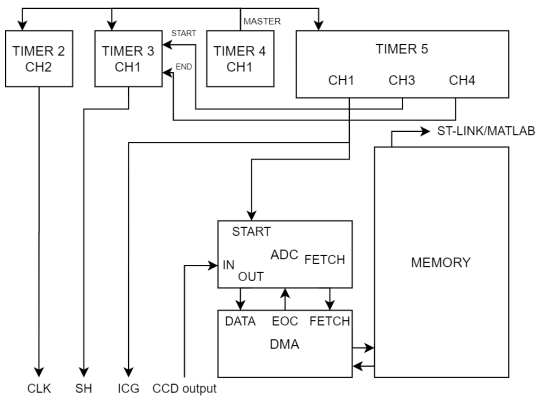

Fig. 7. Block diagram showing the main elements of the software, Timers, ADC, DMA and Memory.

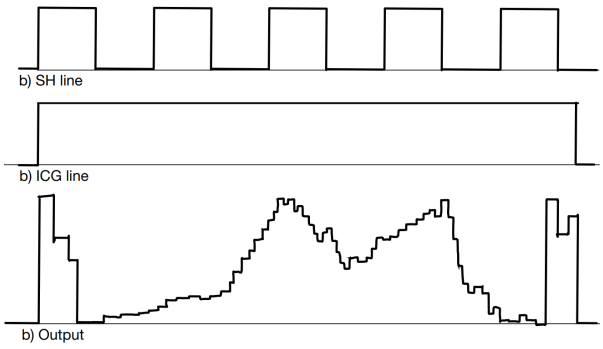

Fig. 8. Scheme showing: a) the SH line as an input to the CCD. b) ICG line delimiting the begin and end of output pixels. c) Illustrative line on the output line OS in the CCD, including dummy and shielded pixels at the beginning and end of the line.

ICG starts and ends the shifting of pixels to the output shift register (inside the CCD package) and CLK is the clock of the CCD. The output pixels start shifting out to the Output pin as soon as the ICG line goes high and the SH line has started oscillating with a period of sh_period. Figure 8 illustrates this process. This period defines the exposure time. The output data rate is one fourth of the clock line. For a clock line of $2\,\mathrm{MHz}$ this translates in a output data rate of $0.5\,\mathrm{MHz}$. The timing requirements of the image sensor are strict, for example, the pulse timing between the ICG and SH line must take place with a delay of $100\,\mathrm{ns}$ to $1000\,\mathrm{ns}$. This suggests that strict synchronization is needed. A functional description of the timers is shown below:

- TIMER2: Outputs a PWM $2\,\mathrm{MHz}$ clock. (CLK)
- TIMER3: Outputs a PWM line with defined period. (sh_pulse) (SH)
- TIMER4: Master timer, clocks all timers.
- TIMER5: Controls ICG line. Period varying depending on exposure. Varies from $3.694\,\mathrm{ms}$ (icg_pulse) being integer multiple of the period of SH. Channel 1 outputs a PWM signal as described in the datasheet [17]. Channel 3 starts counter on Timer2 and Channel 4 stops Timer2.

Table I shows an organized structure corresponding to Timer and Channel, Name, Assigned output PWM line and its period. Note that the parameters x1 and x2 are synchronization parameters that adjust and displace the SH signal in time according in order to meet the timing requirements. The STM32F401RE

Table I. Table showing the timer channels implemented, with its operational name and period in master-clock-cycles.

	Name	Output Assigned	Period (cycles)
T2CH2	Clock	CLK	4
T3CH1	SH	SH	sh_pulse
T4CH1	Master	-	2
T5CH1	ICG	ICG	icg_pulse
T5CH3	SH_dis	-	x1
T5CH4	SH_en	-	x2

inside the board runs at $84\,\mathrm{MHz}$. This clock line (clock line affecting timers: APB1) was pre-scaled to $16\,\mathrm{MHz}$. Inside the master timer it was pre-scaled by a factor of 0.5. The calculation of the length of the counters in clock cycles is based on the output clock of the master timer, which is $8\,\mathrm{MHz}$. If a period of SH = $10\,\mu\mathrm{s}$ is required, a value of 80 for sh_pulse is requried. The calculation formula of time to clock cycles used for adjusting the timers is shown in Equation 3.

$$N_{clocks} = T_{desired} \cdot 8 \cdot 10^6 \tag{3}$$

A repetitive process takes place after one line was shifted to the output pin. All timers go to the original position. This is translated into a constant burst of lines as long as the CCD is ready.

2) Reading and storing lines: The output signal in the output pin is a sample-and-hold type of signal. Although the chip outputs 3694 pixels, only 420 pixels are being read by the ADC, which complies with requisites of already existing finger-vein scanners. In fact the ADC's sampling time is larger than an individual pixel which results in an averaged-pixel. The total accumulated sampling time of all pixel readings covers almost the whole line output. Aliasing is not expected since finger vein images are not high-detailed [5]. This would translate in reading approximately 8.7 pixels in one averaged pixel, therefore an intense change of brightness would have to happen between those 8.7 pixel in order to loose relevant information. Each pixel is $8\,\mu\mathrm{m}$ in width, so a change in 7.7 pixels would mean an object directly above the sensor of $61.69\,\mu\mathrm{m}$. This number exceeds the expected size of visible vascular elements.

One channel of the ADC samples the data from the CCD output as soon as the ICG line goes high. An ADC continuous mode was implemented, i.e. converting each element one after another without any external trigger or interaction. The ADC then samples every 56 clock cycles of $8\,\mathrm{MHz}$ and stores the resulting pixel value on a 8-bit register. Immediately after, the ADC issues a request to the DMA, which counts the number of pixels remaining to transfer and stores this pixel into a memory address in the RAM memory. The process runs until the number of left elements to transfer is zero, therefore completing 420 elements transferred from the ADC to the memory. Once the last element is transfered to the memory, the DMA issues an interrupt request which prevents the ADC from performing more conversions. The resolution of the ADC was

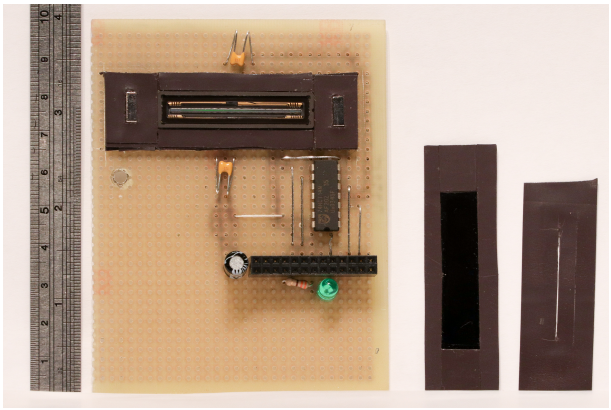

Fig. 9. Image for scale reference showing: (LEFT) The CCD soldered together with a Schmitt trigger and other components. (MIDDLE) The bottom side of the IR filter. (RIGHT) The aperture filter.

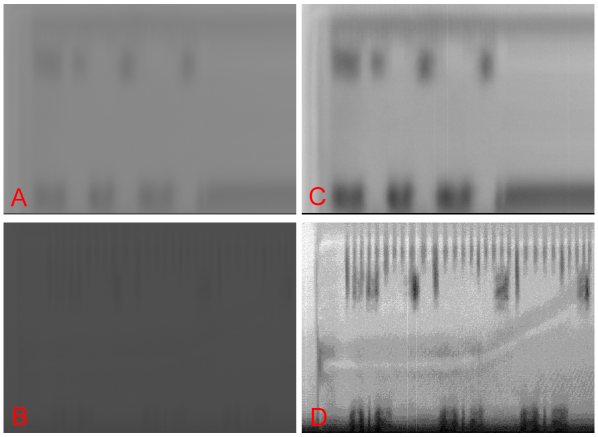

Fig. 10. Image showing a) Ruler swipe under natural light. b) Ruler swipe under natural light with aperture filter. c) Increased contrast version of A for comparison purposes. d) Increased contrast version of B for comparison purposes

set to 8 bits because no noticeable improvement was shown in comparison to 12 bits.

The transmission between the board and pc was implemented through the integrated USB port in the board. This method is asynchronous and the usage of CPU is unknown. Dedicated STMicroelectronics software logs the pixel array on the memory of a PC using the on-board debugger. Matlab then fetches this raw data and builds the whole image line by line. Resulting in a complete PNG-format 2D image.

Another more-efficient communication method was implemented. This method used other channels of the DMA to move data from memory to the USART register synchronously. Leaving the CPU to idle for most of the time. Although this method is much more efficient and enables a two way communication, the required software to perform the acquisition is rather complex, leaving it to further iterations of this project.

V. EXPERIMENTS AND RESULTS

Several experiments were concluded under different scenarios. Almost all scenarios share a common setup, involving an object being dragged perpendicularly on top of the sensor. All experiments are done under a highly dimmed natural light environment unless specified otherwise. Each of the different experiments is done in order to investigate the different characteristics of the prototype that might determine the viability of this technology. Under section V-A, different configurations are described as well as relevant aspects of the testing scheme. Section V-B shows the results and comparisons hand by hand under the described scenarios.

A. Setup for the experiments

Artificial lighting is placed at a distance of approximately $6\,\mathrm{cm}$ whenever implemented. The intensity varies between three values: 10%, 30% , 100%. The speed of the swipe is made handheld, perpendicular to the axis along the line sensor. With the intention of keeping the swipe velocity uniform, two hands were used to move the object to be scanned. To ensure a minimum lateral displacement error (image skewing), guidelines were implemented that constraint the freedom of movement of the object. This does not apply for the actual finger surveys. The $0.5\,\mathrm{mm}$ aperture filter is placed handheld right above the CCD glass, visually aligned.

B. Measurements

Five measurements are made to test contrast, resolution, aperture filter, image smearing, NIR responsivity, detection of bones and veins in phantom fingers and real finger imaging.

1) Contrast, Resolution and aperture filter under different lighting schemes: A cracked ruler was used to prove contrast and resolution of the device under natural lightning (a medium-sized room with only natural light). Figure 10-A corresponds to a simple swipe of the ruler without aperture filter nor NIR filter. It shows resemblance to the actual object, where the numbers are on top and bottom of the image. The image has been rotated to align with the direction of the numbers. The direction of the swipe is from left to right, which holds for all the experiments. Figure 10-B shows the same experiment but with the addition of the aperture filter over the sensor, which results in darker image. By using image processing tools, both of the images in Figure 10-A and 10-B are transformed in a way that lighting levels are similar, producing Figure 10-C and 10-D respectively. It can be seen that the aperture filter improves sharpness in exchange for brightness. Note that the swipe velocities are not equal for both of the experiments, which turns Figure 10-A and 10-C into a slightly more lateral-compressed image.

Figure 11 shows a sharpness comparison between an scan without an aperture filter (11-A) and a scan with an aperture filter (11-B). The brightness is adjusted so lighting levels are similar. This time, a LED lamp was placed directly above the line sensor at a brightness of 30% in order to avoid over exposed areas nor smearing. At first, no big difference is shown. Only when zoomed in, discrepancies arise. Figure 11-C shows a magnified version of 11-A, while Figure 11-D represents a magnified version of 11-B. This comparison suggests that implementing an aperture filter and narrowing the light directivity to only from above, increases sharpness

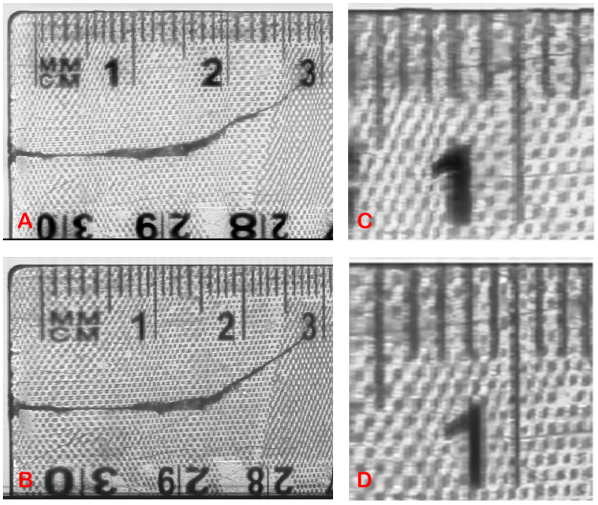

Fig. 11. Image showing: a) Increased contrast version of the ruler swipe under LED light. b) Increased contrast version of the ruler swipe under LED light with aperture filter. c) Partial magnification of A. d) Partial magnification from B.

and definition slightly. A raw version of Figure 11-B is shown in Appendix A.

2) Assessment of light and smearing in bright areas: Smearing causes a whole line to be over exposed when a very bright source of light impacts the sensor. The CCD used suffers from this phenomenon and its effects should be evaluated. Figure 12 shows a comparison between a full smearing (Figure 12-A) and partial smearing (Figure 12-B). In this experiment the NIR LED is placed above the sensor and swiped perpendicularly at a distance of $6\,\mathrm{cm}$. In Figure 12-A an LED at 100% of brightness is shown, causing a horizontal smearing in the direction of the line. The direction of the swipe is up to down. On the other hand, Figure 12-B shows a partial smearing with a partial saturation trail at a brightness of around 10%. In contrast to the experiment performed in A, in experiment B the direction of movement of the LED is not perpendicular to the sensor; it is rotated around a corner of the CCD. In particular, this rotation is done around the z-axis. This rotating effect produces the skewing in the image, converting a circle into an ellipse. Smearing appears to be a

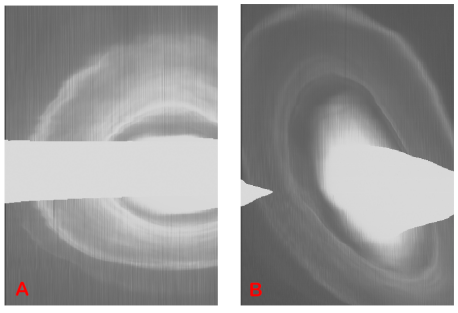

Fig. 12. Smearing caused by the $860\,\mathrm{nm}$ LED on the CCD. In a) a full smearing is produced due to the high intensity of the light source. In b) the light source is reduced and the smearing is partial.

problem when objects that do not cover the whole length of the CCD are scanned. Figure 13 shows this effect on the tip of a finger, where the left side suffers from a saturation trail. Only when the scan reaches the end of the objects it causes these artifacts. The red outline indicates an estimated position of where would the border of the finger be. Anyhow, there are available smearing removal algorithms for CCD imaging sensors [19].

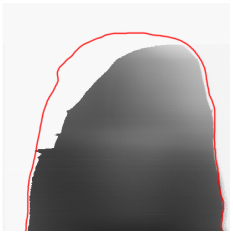

Fig. 13. Smearing at the tip of the finger. The red line indicates the estimated border outline of the finger, not visible due to a saturation trail.

3) Phantom finger experiments: A phantom finger is used together with a NIR led and a IR filter. A phantom finger is a dummy replica of a finger. It has knuckles, bones and veins [20]. It consists of a 3D printed inner plastic imitating a bone, knuckles with materials simulating synovial fluid and veins. This reproduction of a real finger is $2\,\mathrm{cm}$ in diameter and the surrounding tissue is a silicon-based component. Figure 14-A shows a raw composition of a swipe scan of the phantom finger under NIR light. The direction of the swipe is right to left, starting at the west side. Comparing Figure 14-A with 14-B it is possible to correlate the white vertical areas with the knuckles in the visible light image. Also, at the right of the image (representing the tip of the finger) a whiter area can be seen. It is also noticeable that due to the lack of curvature at the top of the finger, smearing and saturation tracks do not appear. Figure 15 shows the swipe of a phantom finger without

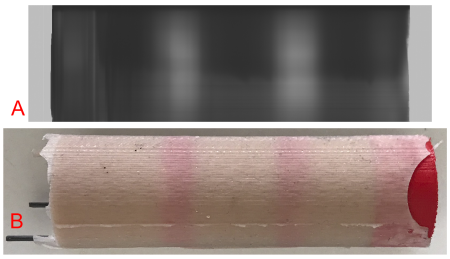

Fig. 14. Visible, NIR and high contrast NIR image. a) Raw NIR swipe of the phantom finger. b) Actual RGB visible image of the phantom finger. c) Increased contrast of A.

knuckles. The swipe is made from left to right. This phantom consists of a inner bone and a horizontal vein, surrounded by tissue. The bone of this phantom ends before the end of the finger takes place, producing a high contrast vertical line. This vertical line can be seen in Figure 15-A and 15-B. This phantom is scanned in reverse, from ”nail” to ”root”, right to left respectively. The ”nail” of this phantom is not visible in this image, instead, an indistinct and disarranged area is visible on the right. This chaotic area is due to the phantom being put in position right after the scan started. The ”vein” of this phantom is placed closest to the sensor, downwards.

Figure 15-B is a higher contrast version of A, post processed in order to ease the visualization of the vein. The vein of this phantom can be seen horizontally as a darker trace.

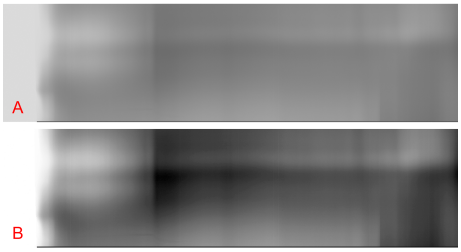

Fig. 15. Swipe scan of a knuckle-less phantom finger. The direction of the swipe is left to right. a) Raw image showing a vein (darker area) horizontally. b) High-contrast version of A.

C. Actual Finger Experiments

A 21 year old male's index finger was used for this experiment. Figure 16 shows four different scans of the same finger together with their higher contrast version. In all of them it is possible to see a lighter area in the middle of the finger, which suggest that the bone is diffusing of the light. The wider areas match the knuckles whereas the darker areas correspond to other tissues. Figures 16-A, 16-B, 16-C and 16-D show a raw image of these 4 scans, while Figures 16-E, 16-F, 16-G and 16-H show post-processed high contrast version. An exposure time of $1/50\,000\,\mathrm{s}$ is applied to all the images in Figure 16. An aperture filter and NIR filter is also used. Finger veins are hardly recognizable in any of these images.

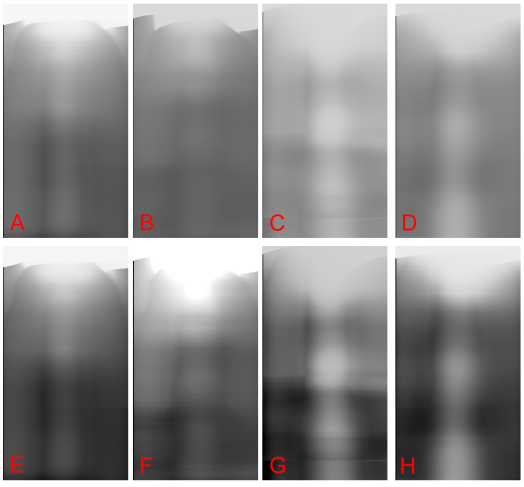

Fig. 16. Different scans of the same finger. Raw images are shown in A, B, C, D and higher contrast images, respectively E, F, G, H.

VI. DISCUSSION AND FUTURE WORK

Some external factors need to be taken into account in order to draw conclusions from the results of the experiments. The first one is the design inaccuracies of the constructed device. The aperture filter was hand crafted with a blade in order to achieve the $0.5\,\mathrm{mm}$ thickness. This leads to an non-uniform aperture line with possible curvilinear characteristics. Also it was hand placed above the sensor. This would be translated into sharpness and definition non-uniformities as well as over or under exposed areas in the images. Even though the aperture filter is not perfect, it is clear from Figure 10-C and 10-D that it increases the sharpness of the images, suggesting that an aperture filter should be implemented for finger vein imaging.

It has to be noted that the brightness of the NIR Light could not be gradually adjusted to a given value, leading to limited lighting possibilities. A logarithmic potentiometer was used but in future iterations PWM-controlled lightning should be implemented. In addition, the vertical and horizontal displacement was prone to movement since a solid construction could not be achieved. This is left for improvement in future research.

Some experiments are hard to perform without the use of a guiding system to keep the flow of the swipe perpendicular to the direction of the sensor, such as the ruler experiment. This is not a limiting factor when it comes to vascular recognition since skewing could be corrected with the appropriate software. Noticeable skewing is not present when scanning real fingers or phantom fingers. Figure 15 corroborates this where the horizontal darker line (which corresponds to the vein) is not largely displaced or skewed.

Figure 11 shows that the resolution achieved is proper in order to map a vein. The resolution goes beyond the requirement under the design criteria of a minimum vein size of $0.5\,\mathrm{mm}$, proving that resolution of this line sensor is satisfactory to reproduce veins. In addition, the sensor proves to perform adequately against image artifacts such as smearing during the experiments using a real finger. The smearing seen in Figure 12 gives a notion of the smearing caused by an infrared LED. Note from Figure 12-B some portion of the right side of the smearing is continued on the left side of the image. It is left to future research to investigate this effect and its impact in finger vein imaging. Smearing and saturation trails do not seem to be a problem when using the phantom fingers since the ends are flat and smearing is not visible. In contrast, it is a problem when imaging the tips of real fingers. Figure 13 shows an obstruction of the finger which suggests that finger tips cannot be imaged accurately. When scanning the whole finger smearing and saturation trails are present on the tip of the finger such as in Figure 16. It has to be noted that finger vein imaging does not focus on finger tips so this smearing is inapplicable.

A full real-time control of exposure time was not implemented, leading to limited results. As a general suggestion, for future software iterations, a two-way communication between PC and board must be implemented, giving flexibility and more possible testing scenarios.

The joints of the bones visible in Figure 16 are optimistic that this technology could be implemented as a vehicle towards flat finger vein recognition. Further research and improvements of this prototype needs to be accomplished in order to deliver an image consisting of veins in the finger. Lastly, Figures 14, 15 and 16 prove the plausibility of this technology.

VII. CONCLUSION

A premature prototype of a flat finger vein imaging device shows promising results. The device is able to identify veins and knuckles in phantom fingers and knuckles in real fingers, appearing as darker or lighter areas. The artifacts and disadvantages of the used Charged Coupled Device do not appear to be an obstacle. There are also no intolerable issues with the resolution and contrast, which have been proved to be sufficient for imaging veins. Although veins are not seen in the images provided by the concluded experiments in real fingers, the viability of this technology as an alternative to already existing technologies has been proven. Partially because phantom fingers show veins and partially because real fingers show joints. Therefore further research and additional iterations of this prototype technology need to take place in order to compete against existing technologies.

APPENDIX A
RAW IMAGE OF RULER SWIPE UNDER LED LIGHT WITH APERTURE FILTER.

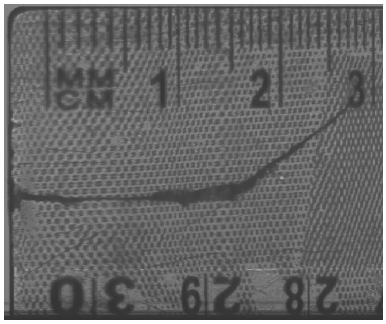

Fig. 17. Raw image of a ruler swipe under visible LED incident light.

APPENDIX B
SIDE VIEW IMPLEMENTATION OF THE FLAT SENSOR.

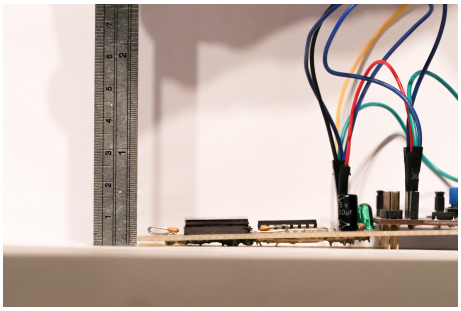

Fig. 18. Side view of the constructed implementation, achieving a height of around1 cm

REFERENCES

[1] M. M. Kassim and A. Sujitha, "Procurepass: A user authentication protocol to resist password stealing and password reuse attack," in *2013 International Symposium on Computational and Business Intelligence*, pp. 31–34, 2013.

[2] F. Z. Glory, A. Ul Aftab, O. Tremblay-Savard, and N. Mohammed, "Strong password generation based on user inputs," in *2019 IEEE 10th Annual Information Technology, Electronics and Mobile Communication Conference (IEMCON)*, pp. 0416–0423, 2019.

[3] M. Verma, R. Sawhney, and R. Chalia, "Biometric based user authentication in smart phones," in *2017 International Conference on Next Generation Computing and Information Systems (ICNGCIS)*, pp. 183–188, 2017.

[4] J. Galbally, S. Marcel, and J. Fierrez, "Image quality assessment for fake biometric detection: Application to iris, fingerprint, and face recognition," *IEEE Transactions on Image Processing*, vol. 23, no. 2, pp. 710–724, 2014.

[5] A. Uhl, C. Busch, S. Marcel, and R. Veldhuis, eds., *Handbook of Vascular Biometrics*, vol. 79 of *Advances in Computer Vision and Pattern Recognition*. Springer, 2020.

[6] H. Ltd., "Hitachi develops a 3mm thin-type finger vein authentication module," 2009.

[7] Jinfeng Yang, Yihua Shi, Jinli Yang, and Lihui Jiang, "A novel finger-vein recognition method with feature combination," in *2009 16th IEEE International Conference on Image Processing (ICIP)*, pp. 2709–2712, 2009.

[8] R. Ramachandra, K. B. Raja, S. K. Venkatesh, and C. Busch, "Design and development of low-cost sensor to capture ventral and dorsal finger vein for biometric authentication," *IEEE Sensors Journal*, vol. 19, no. 15, pp. 6102–6111, 2019.

[9] S. Rozendal, "Redesign of a finger vein scanner," February 2018.

[10] Seung-Min Jung, Jin-Moon Nam, Dong-Hoon Yang, and Moon-Key Lee, "A cmos integrated capacitive fingerprint sensor with 32-bit risc microcontroller," *IEEE Journal of Solid-State Circuits*, vol. 40, no. 8, pp. 1745–1750, 2005.

[11] K. Jang, K. Kim, and K. Jeong, "Fully integrated ultrathin camera for contact fingerprint imaging," in *2019 International Conference on Optical MEMS and Nanophotonics (OMN)*, pp. 10–11, 2019.

[12] F. C. AB., *FINGERPRINTS FPC1080A SWIPE SENSOR*, 2011. Available at https://biometrics.mainguet.org/types/fingerprint/product/FPC/FPC_1080A_flyer.pdf.

[13] P. Johnson and J. Blackstone, "Kids and gender: Differences in exposure and how anthropometric differences could be incorporated computer input device design," pp. 1–7, 05 2020.

[14] G. H. Chapman, R. Thomas, I. Koren, and Z. Koren, "Relating digital imager defect rates to pixel size, sensor area and iso," in *2012 IEEE International Symposium on Defect and Fault Tolerance in VLSI and Nanotechnology Systems (DFT)*, pp. 164–169, 2012.

[15] R. R. Fletcher, V. Raghavan, R. Zha, M. Haverkamp, and P. L. Hibberd, "Development of mobile-based hand vein biometrics for global health patient identification," in *IEEE Global Humanitarian Technology Conference (GHTC 2014)*, pp. 541–547, 2014.

[16] E. N. Pernia and F. Safar, "sapi (simpleapi), a hardware-independent c library for embedded systems programming," in *2017 Eight Argentine Symposium and Conference on Embedded Systems (CASE)*, pp. 1–6, 2017.

[17] T. E. D. . S. CORPORATION, "Ccd linear image sensor: Tcd1304dg - datashet," 2014-2019. Available at https://toshiba.semicon-storage.com/ap-en/semiconductor/product/linear-image-sensors/detail.TCD1304DG.html.

[18] I. P. Limited, "Optolite ir filter - datashet," Available at https://www.instrumentplastics.co.uk/products/optolite-ir-acrylic-infrared-pass-filters.

[19] Y. S. Han, E. Choi, and M. G. Kang, "Smear removal algorithm using the optical black region for ccd imaging sensors," *IEEE Transactions on Consumer Electronics*, vol. 55, no. 4, pp. 2287–2293, 2009.

[20] L. S. P. Normakristagaluh, G.J. Laanstra and R. Veldhuis, "Understanding and modeling finger-vein imaging," in *Understanding and Modeling Finger-vein Imaging*, pp. 4–5, Under preparation for submission.